



Article

Techno-Economic Analysis of a Fuzzy Logic Control Based Hybrid Renewable Energy System to Power a University Campus in Japan

Tatsuya Hinokuma, Hooman Farzaneh *  and Ayas Shaqour 

Interdisciplinary Graduate School of Engineering Sciences, Kyushu University, Fukuoka 816-8580, Japan; hinokuma.tatsuya.617@s.kyushu-u.ac.jp (T.H.); shaqour.ayas.886@s.kyushu-u.ac.jp (A.S.)

* Correspondence: farzaneh.hooman.961@m.kyushu-u.ac.jp

Abstract: In order to reduce the load demand of buildings in Japan, this study proposes a grid-tied hybrid solar–wind–hydrogen system that is equipped with a maximum power point tracking (MPPT) system, using a fuzzy logic control (FLC) algorithm. Compared with the existing MPPTs, the proposed MPPT provides rapid power control with small oscillations. The dynamic simulation of the proposed hybrid renewable energy system (HRES) was performed in MATLAB-Simulink, and the model results were validated using an experimental setup installed in the Chikushi campus, Kyushu University, Japan. The techno-economic analysis (TEA) of the proposed system was performed to estimate the optimal configuration of the proposed HRES, subject to satisfying the required annual load in the Chikushi campus. The results revealed a potential of 2% surplus power generation from the proposed HRES, using the FLC-based MPPT system, which can guarantee a lower levelized cost of electricity (LOCE) for the HRES and significant savings of 2.17 million yen per year. The TEA results show that reducing the cost of the solar system market will lead to a reduction in LCOE of the HRES in 2030.

Keywords: hybrid renewable energy system; fuzzy logic; renewable energy; fuel cell; techno-economic analysis



Citation: Hinokuma, T.; Farzaneh, H.; Shaqour, A. Techno-Economic Analysis of a Fuzzy Logic Control Based Hybrid Renewable Energy System to Power a University Campus in Japan. *Energies* **2021**, *14*, 1960. <https://doi.org/10.3390/en14071960>

Academic Editor: Marco Sorrentino

Received: 26 February 2021

Accepted: 30 March 2021

Published: 1 April 2021

Publisher's Note: MDPI stays neutral with regard to jurisdictional claims in published maps and institutional affiliations.



Copyright: © 2021 by the authors. Licensee MDPI, Basel, Switzerland. This article is an open access article distributed under the terms and conditions of the Creative Commons Attribution (CC BY) license (<https://creativecommons.org/licenses/by/4.0/>).

1. Introduction

1.1. Background and Literature Review

Today, the earth faces a significant environmental problem, which is global warming. Renewable energy is one of the best ways to solve this problem. After the Great East Japan Earthquake, the share of nuclear electricity in Japan has decreased significantly [1]. This is because the public's concern about nuclear power plants has risen due to the nuclear accident. As a result, the dependence on thermal power generation has increased. However, Japan lacks energy resources; its energy self-sufficiency rate is meager compared to that of other OECD countries [2,3].

In 2013, the Japanese government promoted an initiative (3E + S) to achieve energy security, economic efficiency, and environmental compatibility, with safety as a priority [2]. According to this plan, the desirable future energy mix in 2030 is as represented in Figure 1.

As shown in Figure 1, renewable energy is an effective countermeasure to increase energy resilience in Japan. For the current electricity market in Japan, renewable energy sources (RES) utilization mostly focuses on individual power sources, including solar photovoltaic systems, wind turbines, micro-hydropower, etc. However, the big concern with RES is their intermittency due to dependence on uncertain climate conditions [4]. Consequently, reliance on an individual power system can result in over-sizing of the system and also a significant rise in the total cost of the system. The hybridization of variable renewables can allow for smooth, durable, and reliable output to power grids to improve the safety, reliability, and stability of dispatched power, which is cheaper than

investing in single renewable technologies [5–7]. Numerous scholars have focused on optimal designing and planning of the hybrid renewable energy systems (HRES) in Japan. Yoshida and Farzaneh applied the particle swarm optimization (PSO) method to find the optimal configuration of a stand-alone microgrid (Photovoltaic (PV)/wind/battery/diesel) used in providing the required electricity for the residential area in Fukuoka [8]. Takatsu and Farzaneh proposed a hybrid hydrogen-based microgrid, consisting of a biomass supercritical gasifier and a solar water electrolyzer to provide the residential demand load requirement in Shinchi-machi, Fukushima Prefecture [9]. Shaqour et al. proposed an efficient control scheme and design for a hybrid renewable energy system consisting of PV, wind turbine generator, lead-acid battery, inverter, and control unit installed in a typical Japanese house located in Kasuga City, Fukuoka Prefecture [10]. Guohong Wu et al. designed a hybrid microgrid energy system consisting of PV, wind, battery storage, and an electrical double-layered capacitor as secondary battery storage implemented at the Tagajo campus Tohoku Gakuin University, Japan [11]. Sugimura et al. developed a hybrid energy microgrid system consisting of a PV, wind generator, and diesel generator as the primary power sources, with battery energy storage for Aguni Island, located in Okinawa, Japan. They investigated the operation schedule of both the battery system and diesel generator and the optimal system configuration in terms of capacity under the application of demand response programs [12].

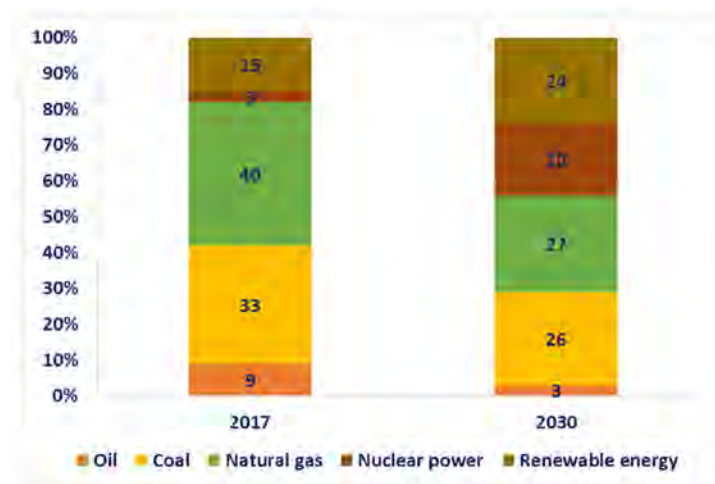


Figure 1. Japan's energy mix outlook in 2030 (Adapted from [2]).

The output power of the proposed HRES varies on environmental variables such as solar irradiance, wind, and operating temperature. The maximum power point tracking (MPPT) control technique is mainly used to extract the maximum capable power of the HRES with respective solar irradiance, wind speed, and temperature at a particular instant of time point.

The MPPT controller will make use of nearly 100% of the available power. In recent years, there has been great interest in the study, improvement, and implementation of MPPT algorithms [13]. MPPT aims to regulate the actual operating voltage of solar panels to the voltage at the MPP. For this purpose, MPPT adjusts the output power of the inverter or DC converter. If the PV output voltage is higher than the maximum power point voltage, then transferred power to the load or network is increased; otherwise, it is decreased. The MPPT methods can be classified into indirect and direct methods. The indirect methods, such as short-circuit and open-circuit methods, need a prior evaluation of the PV panel, or they are based on mathematical relationships or a database not valid for all operating meteorological conditions. Therefore, they cannot obtain exactly the maximum power of a PV panel at any irradiance and cell temperature. Conversely, the direct methods operate at any meteorological condition and act in real time on the voltage reference variable, corresponding to the maximum power provided by the PV system. MPPT can be

realized in the wind power generation control by adjusting the power or torque command. The input of the control block is the rotor speed. The optimum power corresponding to this speed will be generated and will be passed to the outer power control block as the power command. Even though a few improvement methods have just been utilized for MPPT, different and new methods may prompt better outcomes and are suggested for future research. Many algorithms have been developed to efficiently track the maximum power point, such as incremental conductance (INC), hill climbing, or perturbation and observation (P&O) [14]. Zhang et al. proposed a hybrid MPPT algorithm that combines an iterative learning controller (ILC) and P&O to extract maximum power from PV systems. In their research, the ILC was proposed to obtain the maximum power point (MPP) in steady-state operation under periodic long-term variations in irradiance and temperature, where the working power point oscillates near the MPP. A high-frequency P&O was proposed to overcome the ILC's shortcomings under highly changing irradiance, improving the dynamic response under such conditions [15]. Messalti et al. proposed and tested two new artificial neural network (ANN) MPPT controllers based on fixed and variable step size. The neural network was trained based on data collected, using the P&O algorithm for the offline phase of training, configuring the neural network, and using the ANN in a PV system [16]. Ahmed and Salam introduced a modified P&O MPPT algorithm in order to reduce steady-state oscillations and decrease the occurrence of tracking direction errors for the P&O-based MPPT controller. They introduced a modified scheme that dynamically alters the perturbation size coupled with introducing a dynamic boundary condition to prevent divergence from the tracking locus, indicating about 1.1% improvement over the traditional P&O when there is a slow change in irradiance levels and about 12% increase in efficiency under fast irradiance changes [17]. Mei et al. implemented a novel incremental-resistance MPPT with variable step size, addressing the advantages of the ILC-based MPPT. They reported a significant improvement in MPPT response speed and accuracy at the steady-state condition, with an extensive operating range [18]. Sher et al. presented a hybrid MPPT algorithm that combines the fractional short circuit current (FSCC) measurement and the P&O algorithm. The two-stage algorithm proposed increases performance under changing weather conditions, and the reliability of the model under environmental scenarios was satisfactory with both software and experimental validation [19]. Table 1 shows the recent MPPT techniques for PV and wind renewable energy systems.

As mentioned above, although there is substantial research concerning the different MPPT algorithms, there are two challenges with the application of them in HRES:

1. Most of them suffer from the drawback of being slow tracking, due to which the utilization efficiency is reduced.
2. Furthermore, intermittency, rapid irradiation, and temperature changes may cause the MPPT to be oscillating around one of the multiple local peaks of power.

Table 1. A review of recent maximum power point tracking (MPPT) techniques for PV and wind renewable energy systems.

Configuration	Energy Sources	MPPT Technique	Target of Control	Description	Ref
Stand-alone/grid connected	PV-wind	Radial basis function network (RFBN)-based single MPPT.	Boost converter	A single (RFBN)-based single MPPT controller was used to control both boost converters connected to the PV and wind systems, whereas one for each is used in conventional systems. They achieved higher performances over modified (improved) P&O.	[20]
Stand-alone	PV-wind-battery	P&O, FLC, sliding mode control (SMC), hill climbing search (HCS)	Boost converter	A hybrid method of P&O, FLC, and SMC was used for PV MPPT, and a hybrid of HCS and FLC were utilized for wind MPPT. The results show significant performance over conventional P&O, FLC, and robust sliding mode control (RSMC).	[21]

Table 1. Cont.

Configuration	Energy Sources	MPPT Technique	Target of Control	Description	Ref
Stand-alone	PV–battery	Harris Hawk optimization (HHO)	Boost converter	The HHO control was tested under highly varying irradiance, partial shading, complex partial shading, and accurate atmospheric data. It was then compared to PSO, cuckoo search (CS), grey wolf optimization (GWO), and dragonfly optimization algorithm (DFOA), where it showed 10–30% tracking time improvement, and to P&O, where it showed 95.45% steady-state oscillation reduction.	[22]
Stand-alone	PV–wind–battery–fuel cell	Speed-control and single input fuzzy logic (SIFL) controllers	Buck converter	Validated with an experimental setup, the speed-control was used for MPPT to the wind turbine while the SIFL controller was used for PV. A fractional order PID (FOPID) controller was used to control the Bi-directional buck-boost converter for the battery. The results show good potential and performance.	[23]
Stand-alone	PV–wind–battery	Ant colony optimization (ACO)	Buck converter	The ACO MPPT controls a single buck converter for optimizing wind turbine power and battery charging. ACO achieved seven times faster convergence than particle swarm optimization (PSO). A fuzzy logic controller (FLC) was used to control the inverter.	[24]
Grid connected	PV–wind–battery–fuel cell–diesel generator	A hybrid of P&O and Q-Learning (h-POQL)	Boost converter	A combination of the reinforcement learning (RL)-based Q-Learning algorithm and P&O was used for MPPT of the PV system, where it showed improved performance over conventional P&O.	[25]
Stand-alone	PV–battery–fuel cell	Fuzzy sliding-mode controller optimized with water cycle algorithm (WCA)	Boost converter	The WCA was used for the first time in renewable energy systems to optimize the input and output gain of the fuzzy sliding-mode controller. The main target of the control system is to optimize for maximum PV power generation and DC-bus voltage error reduction.	[26]
Grid connected	PV–wind	Adaptive incremental conductance (AIC), modified P&O	Boost converter	A variable step-size AIC was used for MPPT of the PV system, while a modified P&O was used for MPPT of the wind system. The results were validated with accurate monthly weather data.	[27]
Stand-alone	PV	Grey wolf optimized adaptive fuzzy logic controller (AFLC)	Boost converter	GWO was used to optimize the membership functions of the AFLC MPPT controller and was tested on four shading patterns where it overcame the drawback of conventional FLC and P&O MPPT methods.	[28]
Stand-alone	PV	A novel beta parameter-based FLC	Boost converter	A third intermediate beta parameter to the FLC was introduced to reduce the complexity of the fuzzy rule function and cover wider operating conditions reducing the user's dependence on system knowledge.	[29]

Table 1. Cont.

Configuration	Energy Sources	MPPT Technique	Target of Control	Description	Ref
Stand-alone	PV	Bayesian fusion general-purpose adaptive MPPT, PID controller	Boost converter	Bayesian fusion, which is a machine learning-based method, is used to avoid PowerPoint local minima under partial shading cases, while a PID controller is used to minimize steady-state oscillations. Results show enhanced response time and efficiency compared to state-of-the-art techniques.	[30]

1.2. What Will Be Elucidated in this Research

Based on the above discussion, this study aims to introduce a hybrid renewable energy system (HRES) equipped with an advanced MPPT, which is envisioned to be installed at Kyushu University's Chikushi Campus in Kasuga, Japan (Figure 2). To overcome the drawbacks mentioned on the existing tracking systems, such as the P&O method, this study aims at introducing a MPPT system based on fuzzy logic control (FLC), which provides rapid control, and small oscillations once it reaches the MPP, under varying weather conditions. The proposed FLC-based MPPT controls the DC–DC converter, which is connected to the solar panel and wind turbine. The determination of input and output magnitude is the most notable feature of the FLC-based MPPT. The FLC determines the numerical input as a linguistic magnitude based on its own rules. It then selects the linguistic output corresponding to the linguistic information and finally converts it into an output value as a number. Thus, the FLC-based MPPT is faster and more accurate than other MPPT controllers, such as P&O, because it has the flexibility to change the magnitude of the output values depending on the position of the points, resulting in more power output from the HRES.

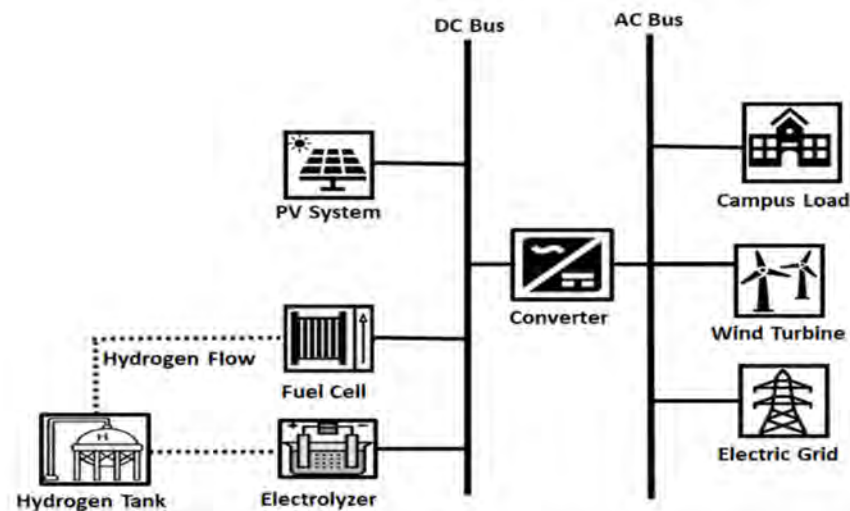


Figure 2. Hybrid renewable energy system (HRES) at the Chikushi campus of Kyushu university.

The research flow diagram in this paper is shown in Figure 3. The first part of this research includes developing a detailed dynamic simulation performed in MATLAB Simulink to simulate the technical performance of the PV arrays and wind turbine, which are equipped with the FLC-based MPPT. The Simulink is used to evaluate the effectiveness of the FLC-based MPPT in rapid tracking of the MPP and extracting surplus power from the HRES, compared with a conventional P&O-based MPPT. The detailed meteorological data used in this study are collected from the Japan Meteorological Agency for Fukuoka City.

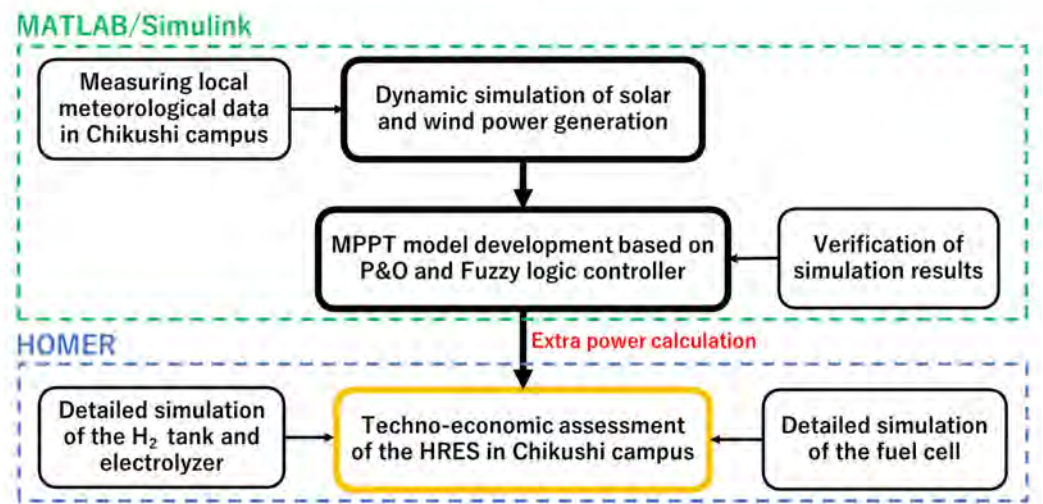


Figure 3. Research flow in this paper.

The second part of the study discusses a detailed techno-economic analysis (TEA) of the proposed HRES, including the hydrogen production and storage components. TEA is used to find the optimal configuration of the HRES and verify the balance of electricity and hydrogen generation for securing the operation feasibly during the system’s lifetime. Furthermore, it addresses the role of the FLC-based MPPT in reducing the levelized cost of electricity (LCOE) of the proposed HRES and, finally, the impact of the future costs of each component (solar, wind, fuel Cell) on the LCOE in 2030 will be evaluated.

2. Model Development

2.1. Solar Power Simulation Model

Figure 4 shows the whole solar-module Simulink model, including FLC–MPPT systems. The technical specification of the solar panel used in this study is given in Table 2. Figure 5 shows the schematic diagram of the buck converter. The DC–DC converter is used as an impedance matching system to track the MPP. The buck converter switches ON and OFF to adjust the output voltage by referring to the duty cycle from the MPPT, following the MPP voltage.

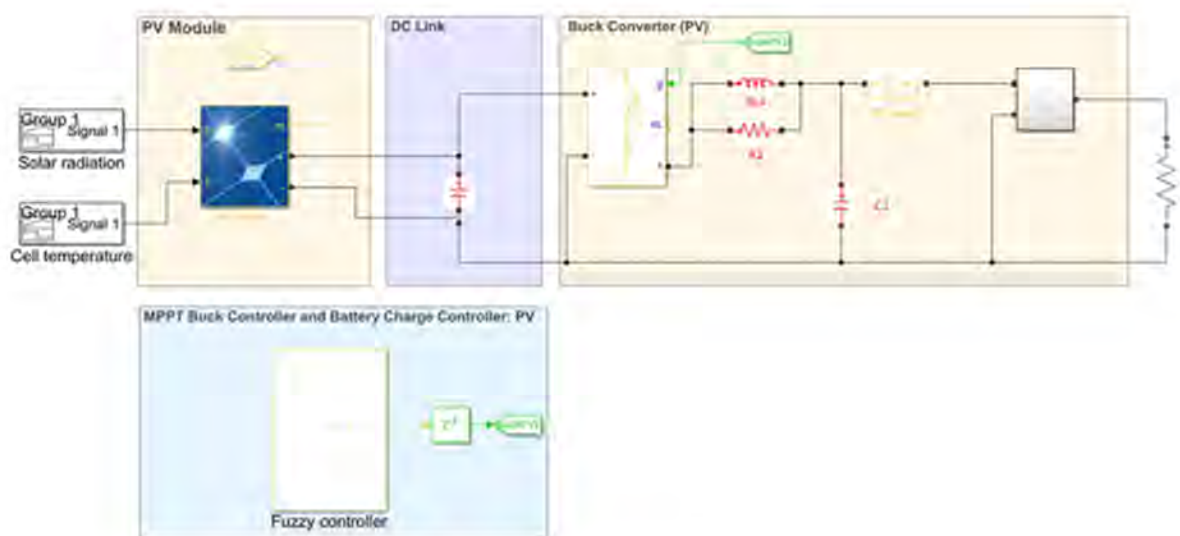


Figure 4. PV Simulink model.

Table 2. Technical specifications of the solar panel [31].

Parameter	Value
Maximum Power [W]	160
Voltage at MPP [V]	17.9
Current at MPP [A]	8.94
Open circuit voltage [V]	21.6
Short circuit current [A]	9.47
Temperate coefficient of I_{sc} ¹ [%/°C]	0.10 ± 0.01
Temperate coefficient of V_{oc} ² [%/°C]	$-(0.38 \pm 0.01)\%/^{\circ}\text{C}$
The number of cells on the PV panel	36

¹ Short-circuit current. ² Open circuit voltage.

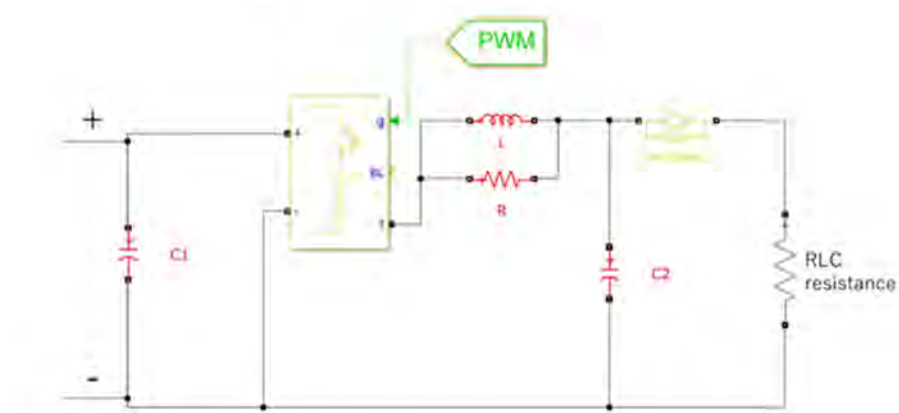
**Figure 5.** Schematic diagram of the buck converter.

Table 3 shows the technical parameters of the buck converter. In this buck converter, an insulated-gate bipolar transistor (IGBT) buck converter is connected to each PV panel. The pulse width modulation (PWM) is controlled by combining IGBTs and diodes, followed by inductors, freewheeling diodes, and capacitors.

Table 3. Parameter of the buck converter [10].

Parameter	Value
Capacitance (C1)	2.2 [mF]
Capacitance (C2)	2.2 [mF]
Resistance (R)	$10,000 \times 10^3$ [Ω]
Inductance (L)	3 [mH]

Fuzzy logic is a type of multi-valued logic that can express linguistic variables by using values from 0 to 1, similar to human thinking. The fuzzy logic controller comprises three components: fuzzification, rule interface, and defuzzification, as shown in Figure 6.

In the stage of fuzzification, numeric input variables are transformed into linguistic variables. Typically, the input variables of the controller are the error (E) and the variation of error (CE). The error shows the operating point of the PV system concerning the MPP, where it should be zero, and its variation shows how this point moves in the power-voltage curve. The transformation is carried out by applying the membership functions set for different input variables ranges, and its value varies between 0 and 1. The interface is responsible for implementing the rule-based functions that define the behavior of the controller. The controller output will be a linguistic variable that establishes the duty ratio

of the converter and iteratively makes the error tend to zero. In the defuzzification stage, the membership functions are applied to obtain the numerical output values.

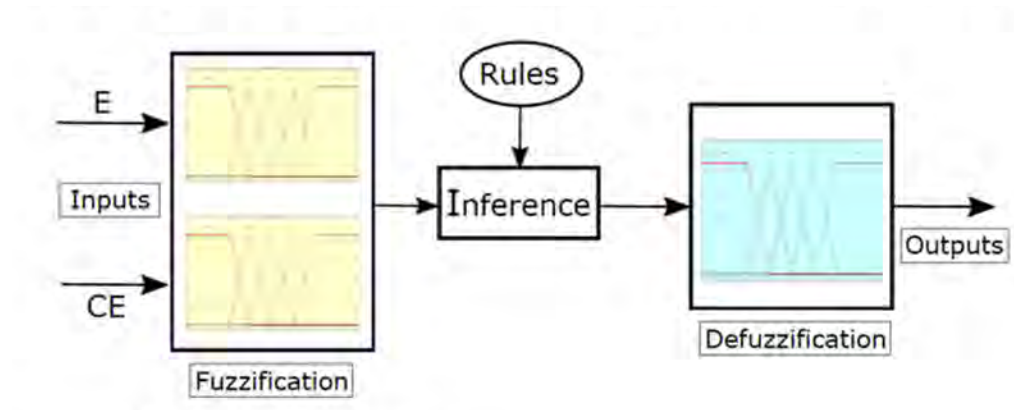


Figure 6. Structure of fuzzy controller.

The FLC judges the operating point (OP) position by using two inputs. These are the slope of the power–voltage (P–V) curve’s tangential line ($\frac{dP}{dV}$) and displacement direction of the operating point ($\frac{d^2P}{dV^2}$), which are shown in Figure 7.

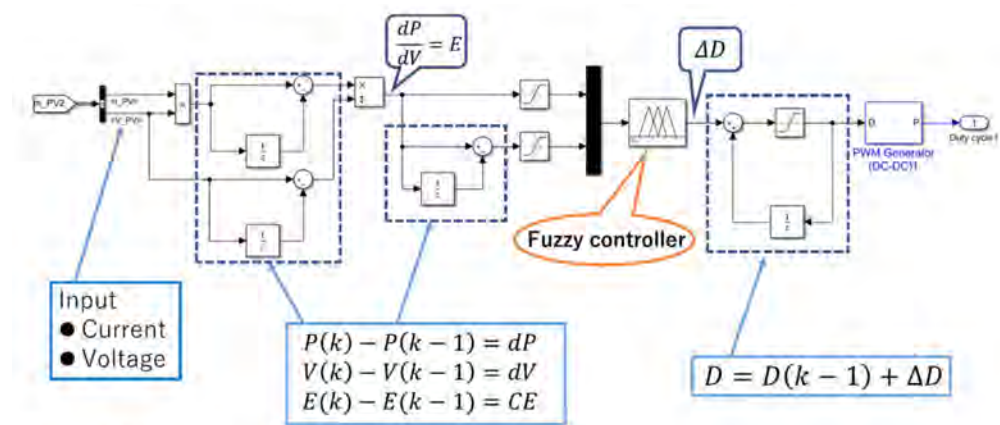


Figure 7. PV fuzzy controller Simulink model.

The FLC judges the MPP position by using two inputs. These are the slope of the P–V curve’s tangential line ($\frac{dP}{dV}$) and displacement direction of the operating point ($\frac{d^2P}{dV^2}$). These two inputs are expressed following equations, respectively.

$$E(k) = \frac{P(k) - P(k - 1)}{V(k) - V(k - 1)} \tag{1}$$

$$CE = E(k) - E(k - 1) \tag{2}$$

where, $P(k)$ and $V(k)$ are the power and voltage of the PV panel at sample time k .

These input values are converted to the linguistic variables through membership functions. Figures 8 and 9 show the membership functions for input values in this research. Linguistic variables are divided into five categories: NB (negative big), NS (negative small), ZE (zero), PS (positive small), PB (positive big).

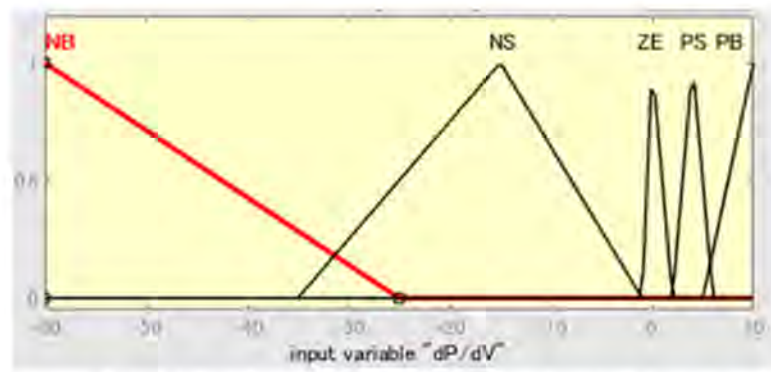


Figure 8. PV fuzzy logic control (FLC) membership function for E [19].

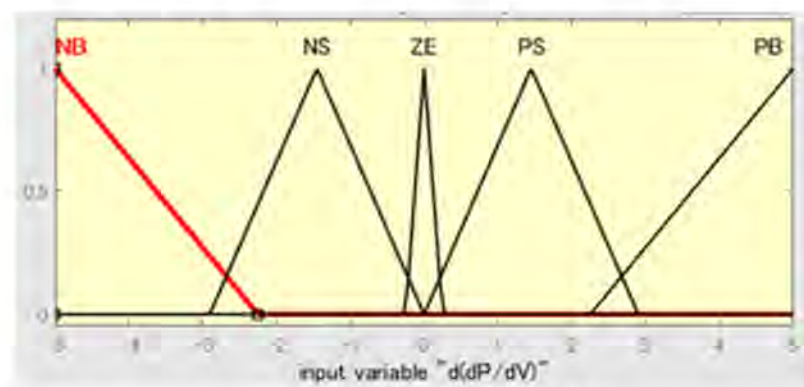


Figure 9. PV FLC membership function for CE [32].

Table 4 shows the fuzzy rule used in this research [33]. These 25 rules determine fuzzy outputs. In the power–voltage curve, there are three regions, as shown in Figure 10. In region ①, $E(k)$ is positive. This indicates that the operating point is on the left side of the MPP. To reach the MPP, the duty ratio should be decreased. For example, when $E(k)$ is PS and $CE(k)$ is NS, it means OP is approaching MPP from the left side. At this time, the fuzzy controller outputs ZE not to make oscillations. In region ②, $E(k)$ is zero, and OP is close to MPP. When $CE(k)$ is NB, the OP is moving towards the right side. And the controller outputs PS to stop the OP from moving. In region ③, $E(k)$ is negative. When $CE(k)$ is negative, the OP is getting away from MPP towards the right side. At this stage, the controller increases the duty cycle to bring the OP closer to MPP. Finally, the outputs (ΔD) from the fuzzy controller are converted into numerical values, as shown in Figure 11, and duty cycle $D(k)$ is calculated by the following equation:

$$D(k) = D(k - 1) + \Delta D \tag{3}$$

Table 4. Fuzzy rules for the PV panel.

E	CE				
	NB	NS	ZE	PS	PB
NB	ZE	PB	PB	PB	PB
NS	PB	PB	PS	ZE	ZE
ZE	PS	ZE	ZE	ZE	NS
PS	ZE	ZE	NS	NB	NB
PB	ZE	NB	NB	NB	ZE

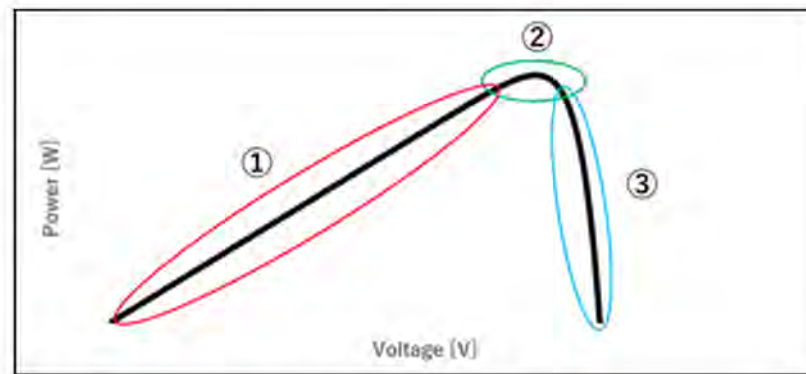


Figure 10. Power –voltage curve of the PV panel.

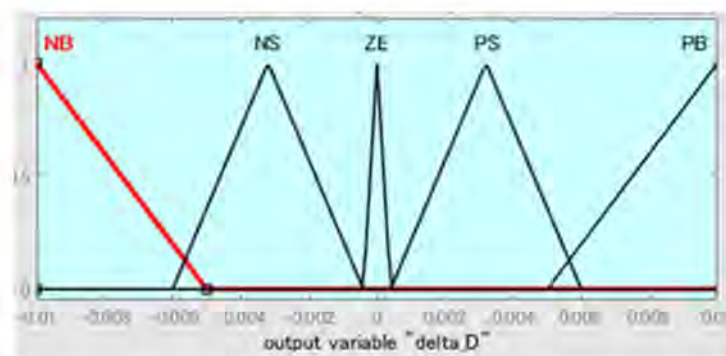


Figure 11. Output membership function for ΔD [19].

2.2. Wind Power Simulation Model

Figure 12 shows the wind turbine generator in the Simulink model, which consists of the wind turbine itself, back converter, and MPPT controller. A battery is also connected to the load part in parallel in order to keep the voltage applied to the load constant and prevent errors that may occur during the simulation. The technical specification of the wind turbine generator used in this simulation is shown in Table 5. Figure 13 shows the MPPT controller's details, where the fuzzy controller determines the appropriate output value ΔD . The following equations represent inputs for the fuzzification in the wind turbine.

$$E(k) = P(k) - P(k - 1) \quad (4)$$

$$CE(k) = V(k) - V(k - 1) \quad (5)$$

$$D(k) = D(k - 1) + \Delta D \quad (6)$$

Table 5. Wind generator parameters [10].

Parameter	Value
Rated power	400 W
Rated voltage	12 V
Start-up wind speed	2.5 m/s
Rated wind speed	10.5 m/s
Maximum wind speed	35 m/s
Rated rotation speed	800 rpm
Fan blade quantity	3
Rotor blades diameter	1.2 m

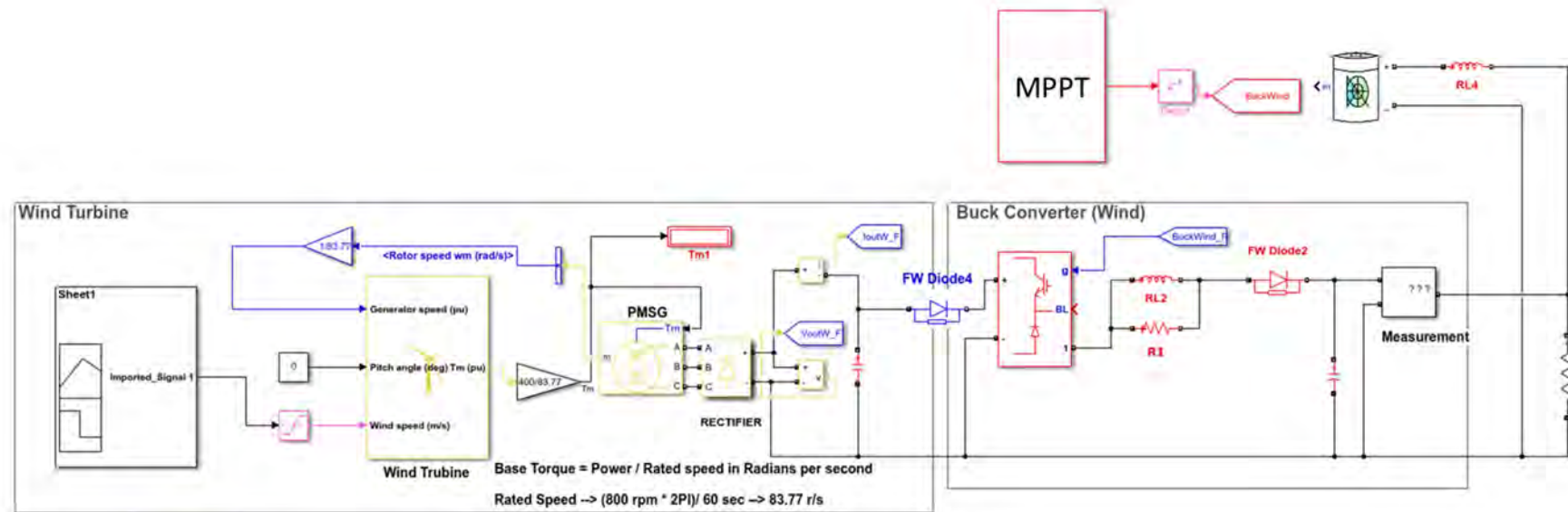


Figure 12. Wind generator Simulink model.

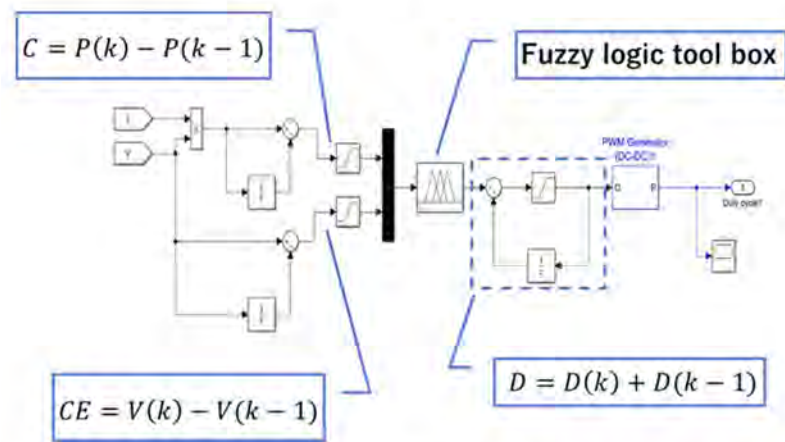


Figure 13. Simulink model of the fuzzy controller for the wind generator.

Table 5 represents the fuzzy rules that are used in the wind turbine MPPT system.

Figures 14–16 show membership functions for $E(k)$, $CE(k)$ and ΔD , respectively. Table 6 represents the fuzzy rules.

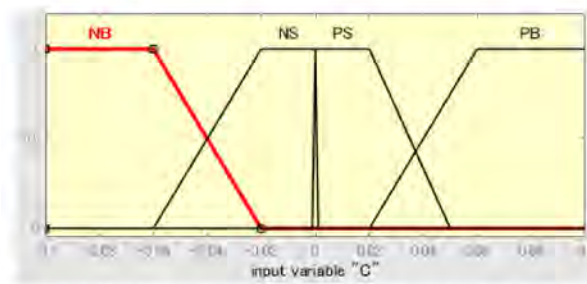


Figure 14. Wind turbine FLC input membership for C.

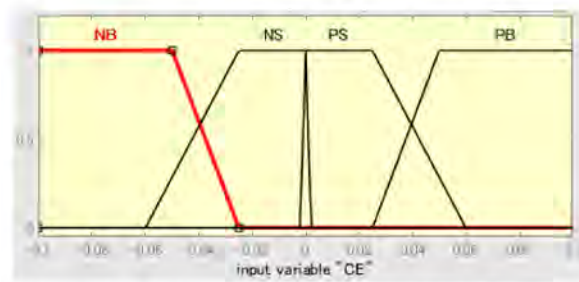


Figure 15. Wind turbine FLC membership for CE.

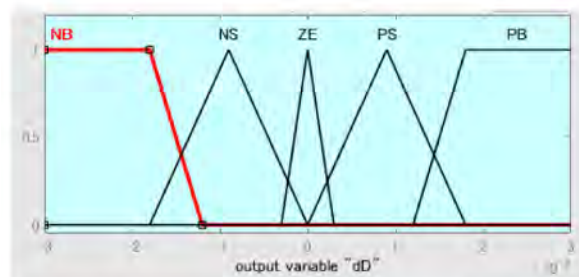


Figure 16. Wind turbine FLC output membership function for ΔD .

Table 6. Fuzzy rules for the wind turbine.

E	CE				
	NB	NS	PS	PB	
NB	NB	NS	PS	PB	
NS	NS	NS	PS	PS	
PS	NS	ZE	ZE	PS	
PB	NS	ZE	ZE	PS	

3. Experimental Setup

Figure 17 shows the proposed HRES, which is installed at the campus in Kasuga City, Fukuoka Prefecture, Japan [9]. The proposed system consists of three PV modules with a total power of (480 W), a wind turbine (400 W), a lead-acid battery (30 Ah), an inverter, and a MPPT controller, which operates based on the P&O method.

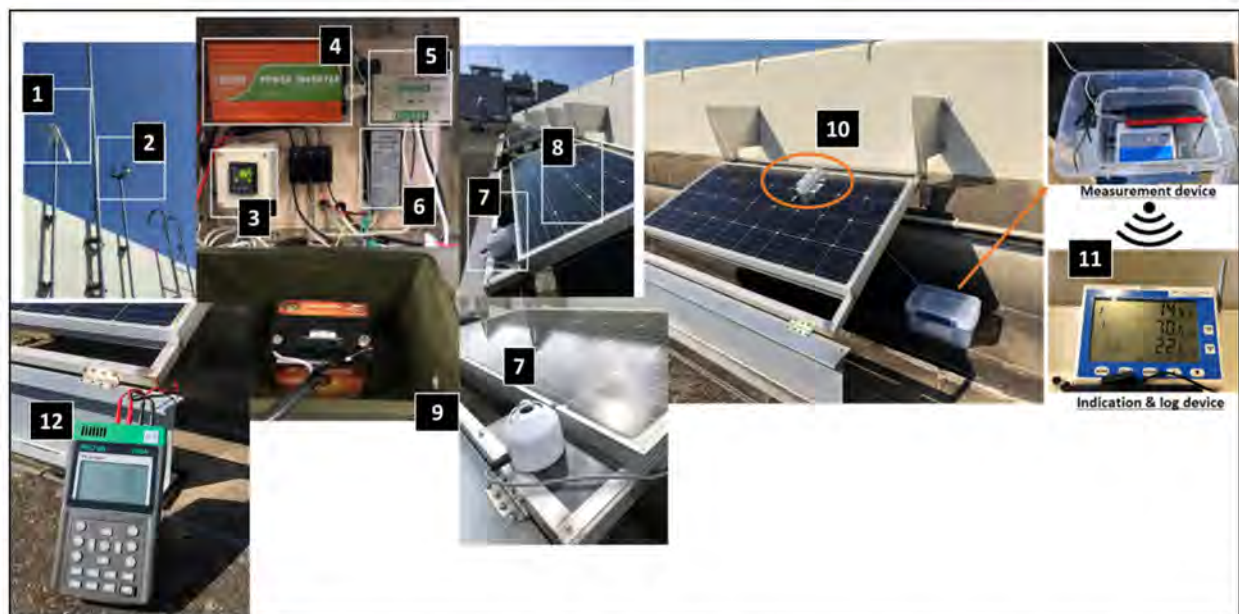


Figure 17. Experimental setup in this study: (1) wind turbine, (2) weather measurement station, (3) power datalogger, (4) inverter, (5) PV DC converter and MPPT controller, (6) wind DC converter and MPPT controller, (7) MS-40C pyranometer, (8) PV modules, (9) battery, (10) LM335 thermocouple, (11) temperature datalogger, (12) solar analyzer PROVA 200A.

The solar panel surface temperature was measured by using a LM335 temperature sensor, which was installed on the surface of the panel. The incident solar radiation on the PV panels was measured, using an MS-40S pyranometer. The solar analyzer (PROVA 200A) was used to measure the short-circuit current and open voltage of the solar panel and extract the current-voltage curves under the various solar irradiations and ambient temperatures.

4. Results and Discussions

4.1. Comparison between the FLC-Based and P&O-Based MPPT Systems

The simulation model was carried out, considering a sunny, cloudy, and rainy day in each month (see Table 7). Figure 18 shows the comparison between the P&O-based and the proposed FLC-based MPPTs in this research for a short period of 10 min simulation on this sunny day. As shown in this figure, the FLC-based MPPT extracts higher power with lower oscillation than the P&O controller. The better performance of the FLC is more evident at the higher levels of solar irradiation. The simulation results reveal that the output power based on the FLC-based MPPT is significantly higher than the P&O-based MPPT on cloudy

days. This is because the P–V curve slope is extremely small due to the low solar radiation (see Figure 19).

Table 7. Selected dates for testing the simulation model in this study.

Sunny Day	Cloudy Day	Rainy Day
1-Jan	13-Jan	22-Jan
4-Feb	7-Feb	12-Feb
20-Mar	22-Mar	28-Mar
14-Apr	15-Apr	19-Apr
1-May	25-May	26-May
8-Jun	4-Jun	25-Jun
16-Jul	17-Jul	6-Jul
29-Aug	28-Aug	7-Aug
14-Sep	20-Sep	12-Sep
20-Oct	8-Oct	22-Oct
5-Nov	19-Nov	18-Nov
12-Dec	29-Dec	22-Dec

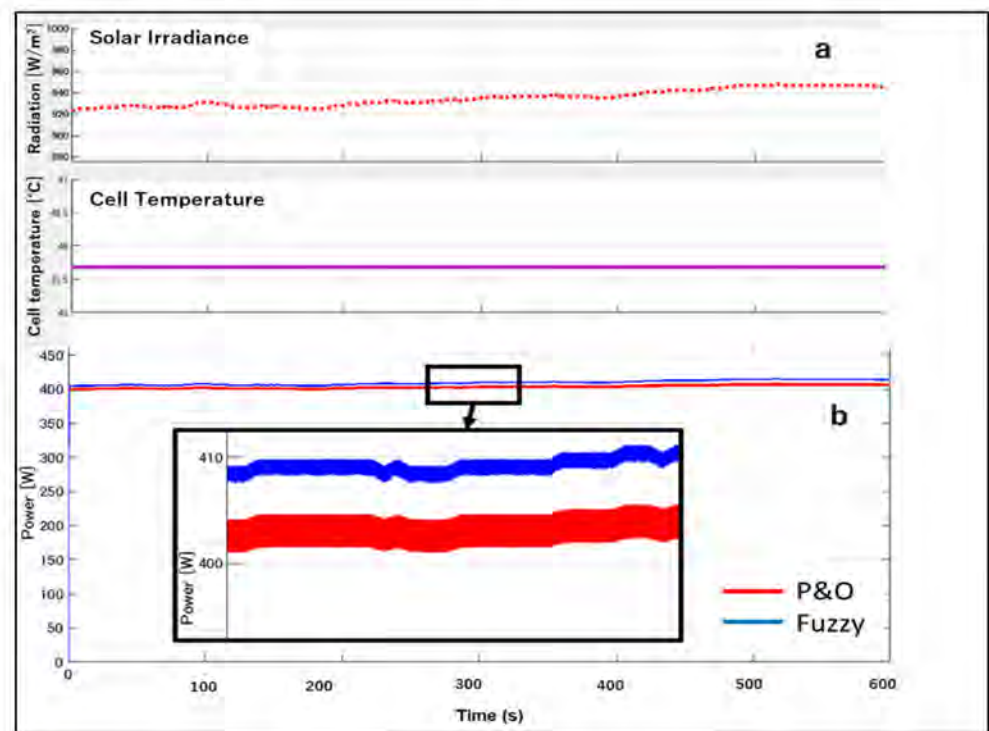


Figure 18. Comparison between the FLC-based and perturbation and observation (P&O)-based MPPT systems for PV (sunny day): (a) Weather conditions; (b) Output power.

The deviation from the P&O-based MPPT appears during the fast-changing environmental conditions, such as rapid changes in solar irradiation or ambient temperature, which is basically due to its lower tracking speed, especially when the variation of power caused by the different intensity of irradiation is larger than the one produced by the perturbation. Compared with the FLC-based MPPT, the fixed step-size perturbation applied to the P&O-based MPPT cannot satisfy both dynamic and steady-state response conditions,

since big perturbations provide a rapid reach of MPP, but also cause large oscillations. On the other hand, small changes remove these oscillations but give a slow performance to the MPPT. Furthermore, partial shading can cause the MPP tracker to be oscillating around one of the multiple local power peaks. Another drawback of the P&O-based MPPT is that it cannot recognize the difference between local and global MPP. Therefore, the expected output power is lower than the FLC-based MPPT.

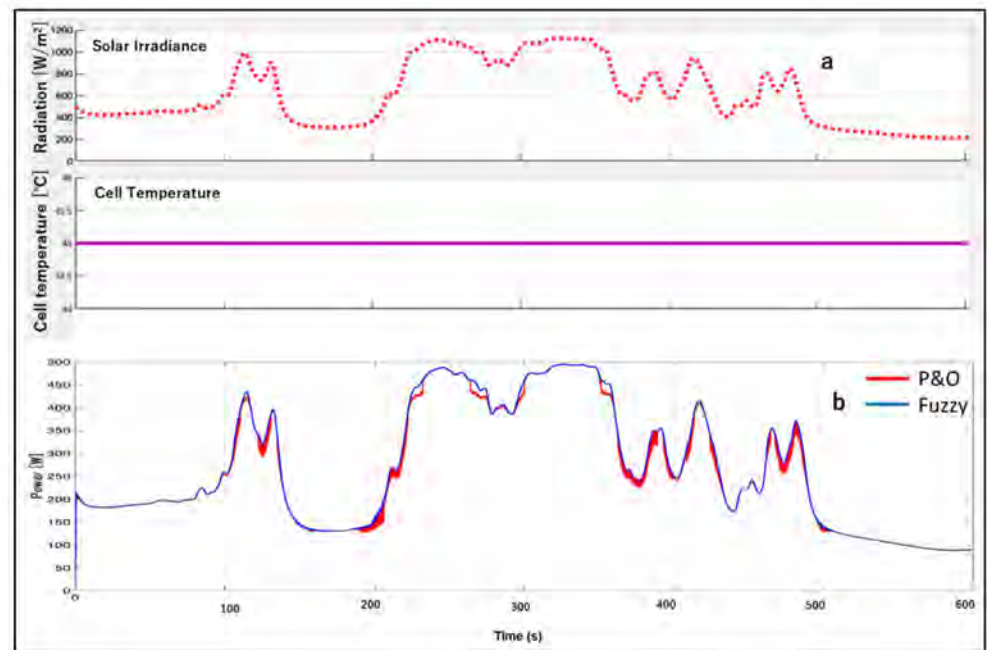


Figure 19. Comparison between the FLC-based and P&O-based MPPT systems for PV (cloudy day): (a) Weather conditions; (b) Output power.

Figure 20 shows the comparison between the FLC-based and P&O-based MPPTs for the wind turbine on 1 April 2020. As shown in this figure, there are almost no differences between fuzzy and P&O controller results for the wind power generator. Although the proposed FLC offers excellent performance in controlling solar panels, it doesn't significantly improve the wind turbine's maximum power, particularly at low wind speed. This is because the wind control system includes mechanical (pitch control) and electrical power sections, but only the electrical part was considered in the simulation model.

The simulation results for an entire period of one year are reported in Table 8. The results revealed a potential of 2% extra power generation from the proposed HRES, using the FLC-based MPPT system. According to the results, by implementing the FLC-based MPPT system, about 26.2 kWh/y excess electricity can be extracted from each kW installed capacity of solar panels in the Chikushi campus.

4.2. Techno-Economic Analysis of the Proposed HRES

HOMER Pro is used for the techno-economic analysis in this research. HOMER software was developed by NREL (National Renewable Energy Laboratory). This software enables the optimal design and sizing of hybrid renewable energy systems by performing a techno-economic analysis of off-grid and grid-connected power systems [34]. HOMER considers two economic indicators, net present cost (NPC) and levelized cost of energy (LCOE). The total NPC of a system is the present value of all the costs the system incurs over its lifetime, minus the present value of all the revenue it earns over its lifetime. Costs include capital costs, replacement costs, O&M costs, fuel costs, emissions penalties, and the costs of buying power from the grid. Revenues include salvage value and grid sales revenue. HOMER calculates the total NPC by summing the total discounted cash flows

in each year of the project lifetime [35]. The formula for calculating NPC is expressed as follows:

$$NPC = I + \sum_{i=1}^n (C_y) \left[\frac{1}{(1+d)^i} \right] \quad (7)$$

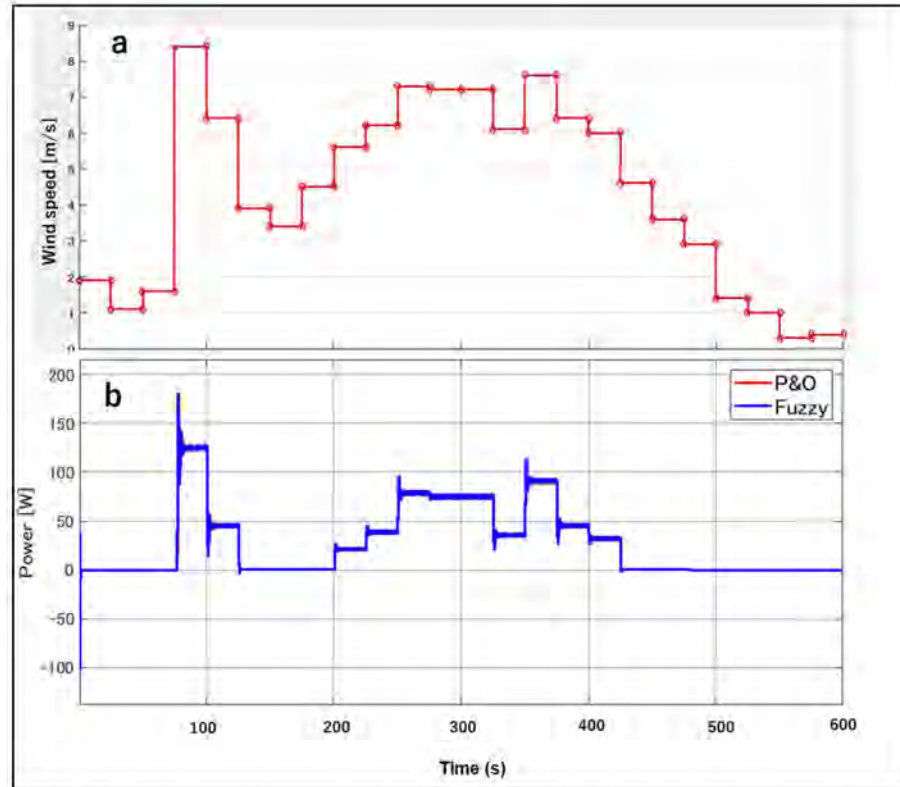


Figure 20. Comparison between the FLC-based and P&O-based MPPT systems for the wind turbine (windy day); (a) Wind speed; (b) Output power.

Table 8. Surplus output power from the FLC-based MPPT compared to the P&O-based MPPT.

Month	P&O Power [kWh]	Fuzzy Power [kWh]	Power Difference [kWh]	Saving [%]
January	33.41	34.16	0.76	2.27
February	38.55	39.37	0.82	2.13
March	52.92	54.47	1.55	2.94
April	66.05	67.92	1.87	2.83
May	62.33	63.73	1.40	2.24
June	66.27	67.54	1.27	1.92
July	26.20	26.57	0.37	1.42
August	54.01	55.02	1.01	1.86
September	52.68	53.91	1.24	2.35
October	59.61	60.69	1.07	1.80
November	49.67	50.59	0.92	1.84
December	15.79	16.09	0.29	1.86
Total	577.49	590.06	12.57	2.18

The $LCOE$ is defined as the average cost per kWh of electrical energy produced by the system, as follows:

$$LCOE = \frac{C_{ann,tot}}{E_{served}} \quad (8)$$

where:

I : Initial capital cost [JPyen]

n : Project span [year]

C_y : Yearly cost (O&M and replacement) [JPyen]

d : Discount rate [%]

E_{served} : Total electrical served [kWh/year]

$C_{ann,tot}$: Total annualized cost of the system [JPyen/year]

Figure 21 represents the proposed grid-tied system, including solar PV, wind turbines, fuel cells, electrolyzers, and hydrogen tanks, as shown in the (FC: Fuel cell, WT: Wind turbine). All renewable energy systems are connected to the DC bus, and the electrolyzer uses only electricity supplied by solar and wind power to electrolyze water and produce hydrogen. The AC bus is connected only to the grid, and the electricity provided by the power company is used solely for power consumption on campus. Figure 22 shows the average hourly power consumption, maximum and minimum power consumption for each month at the Chikushi campus. When considered throughout the year, the average total daily power consumption is estimated at 25,256 kWh/day, and the total annual power consumption is about 9218.5 MWh/year.

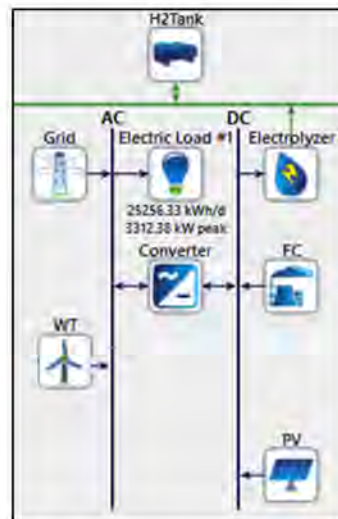


Figure 21. HOMER simulation model of the proposed HRES.

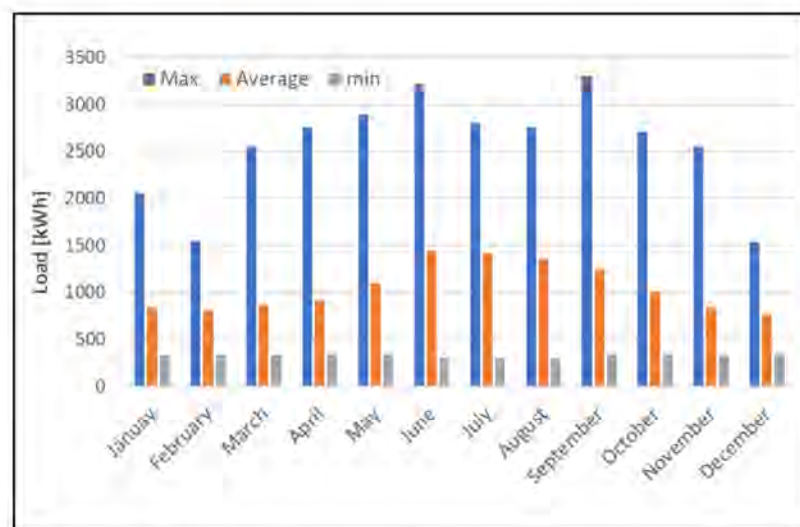


Figure 22. Monthly average electricity consumption in Chikushi campus, Kyushu University, Japan.

In this study, the wind turbine size is limited in the range of 0 to 10 kW. This is because the campus site area where the HRES will be installed is restricted, and wind turbines require more land than any other renewable energy system. The installed capacity of the hydrogen system is considered as: 1 kW (Fuel cell): 10 kW (Electrolyzer): 1 kg (H₂ tank). This is based on the assumption that the electrolyzer operates for 9 h during the day to produce hydrogen, and the fuel cell consumes the stored hydrogen for 7 h after sunset. The electrolyzer's power consumption is assumed about 46.4 [kWh] per 1 kg of hydrogen.

Table 9 shows the current estimated costs for each component and economic data. The costs are divided into initial capital cost, operation and maintenance (O&M) cost, and replacement cost. Besides this, the purchase price of electricity was considered to be 22 JPYen/kWh [8].

Table 9. Costs items of the main components of the proposed HRES.

Component	Lifetime [years]	Initial capital cost [JPYen]	Replacement [JPYen]	O&M [JPYen/year]	Reference
PV [kW]	20	230,000	230,000	P&O: 11,500 Fuzzy: 10,924	[8]
WT [kW]	20	250,723	250,723	7740	[7]
Fuel cell [kW]	10	400,000	400,000	9000	[8]
Electrolyzer [kW]	10	170,000	170,000	3000	[8]
H ₂ tank [kg]	20	150,000	150,000	4000	[8]
Inverter [kW]	20	13,970	13,970	110	[7]
Parameter		Values			
Nominal discount rate [%]		0.3			
Expected inflation rate [%]		0.98			
Project lifetime [years]		20			

It is noted that the economic benefit from surplus power generated by the FLC-based MPPT is monetized as a reduction in O&M cost. As shown before, for each 1 kW of installed capacity of the PV, about 26.2 kWh surplus electricity can be generated from the FLC-based MPPT system.

4.2.1. Base Case Scenario

The simulations were performed for ten different fuel cell sizes from 10 kW to 100 kW at 10 kW intervals. The capacity of each component, except the hydrogen system, is determined by HOMER optimization. The simulation results show that the best COE for both P&O and the fuzzy controller is obtained when the smallest fuel cell of 10 kW is used. Tables 10 and 11 show the breakdown of HRES and cost analysis results for the FLC-based and P&O-based MPPTs.

Table 10. Component capacity and electricity production of the proposed HRES.

Component	P&O-Based MPPT		FLC-Based MPPT	
	Size [kW]	Electricity Production [MWh/Year]	Size [kW]	Electricity Production [MWh/year]
PV	1675	2350	1782	2500
Wind turbine	10	14.5	10	14.5
Fuel cell	10	4.26	10	4.6
Electrolyzer	100	54.1	100	−58.3
H ₂ tank	20	—	20	—
Converter	1492	—	1542	—
Grid purchase	—	7253	—	7144

Table 11. Cost analysis comparison of the FLC-based and P&O-based MPPTs.

Controller	NPC [JPYen]	Cost Of Electricity [JPYen]	Operating Cost [JPYen/Year]	Total O&M [JPYen]	Initial Capital [JPYen]
P&O	4.31 B	38.09	180 M	3.86 B	433 M
Fuzzy	4.29 B	37.74	178 M	3.81 B	458 M
Difference	21.4 M	0.342	2.17 M	46.7 M	−25.3 M

According to the base case scenario, the FLC-based HRES enables the installation of more PV systems than the P&O-based system. With the increase in PV system generation, the energy supply to the electrolyzer also increases. This means that the fuel cell in the FLC-based HRES generates more electricity than the P&O-based system. Furthermore, the FLC-based HRES shows better cost benefits.

4.2.2. Future Cost Scenario

This scenario discusses the cost analysis of the HRES components based on their future prices. Table 11 summarizes the initial capital costs in 2020 and expected costs in 2030 for solar panels, wind turbines, fuel cells, and electrolyzers. Over the past few years, the amount of renewable energy plants installed has increased dramatically due to the policies, research and development, and funding of each major country. Among them, solar power is considered to be one of the most competitive technologies. The total installed cost has decreased by 74% between 2010 and 2018. For the case of wind power, improvements in technology and manufacturing processes, as well as the rise of competitive supply chains, are driving down the price of installation costs; average prices in 2018 ranged from 790 to 900USD/kW, down from 910 to 1050 USD/kW in 2017. In 2017, the Japanese government established the Strategic Roadmap for Hydrogen and Fuel Cells, the world's first national hydrogen strategy. Specifically, it aims to achieve hydrogen costs comparable to gasoline and LNG costs, along with a reduction in the cost of installing fuel cells and electrolysis equipment [36]. Based on the cost projections in Table 12, the following three scenarios were considered for the proposed FLC-based hybrid system.

Table 12. Summary of current and future initial capital costs in the future cost scenario.

Component	2020 [JPYen]	2030 [JPYen]
PV [kW]	230,000	91,740 [5]
WT [kW]	250,723	187,000 [5]
Fuel cell [kW]	400,000	300,000 [6]
Electrolyzer [kW]	170,000	50,000 [6]

- Scenario (1): future costs are only applied to solar panels;
- Scenario (2): future costs are only applied to fuel cells and electrolyzers;
- Scenario (3): future costs are applied to all components.

Table 13 represents the respective values of cost of electricity (COE) based on the above scenarios, taking into account the various sizes of the cells from 10 kW to 100 kW. The lowest COE can be achieved with a 10 kW fuel cell in all scenarios. The best results are obtained in scenario (3).

Table 14 shows the component sizes of each RES for different classes of (A) through (D). It can be seen that all the component sizes of class (C) are the same as the class (A), and there is not much difference in the COE, even though the installation cost of the hydrogen system is decreasing. This is because the hydrogen system is only powered by the PV system. As long as PV system installations do not increase due to falling PV panel installation costs, the amount of electricity generated by the fuel cell will not increase, and the share of HRES in the total electricity will not change. In addition, class (D) has

the most extensive size of the hydrogen system and the largest solar panels to provide its electricity supply.

Table 13. Summary of cost of electricity (COE) for each model in the future cost scenario.

Scenario	Fuel Cell Size									
	10 kW	20 kW	30 kW	40 kW	50 kW	60 kW	70 kW	80 kW	90 kW	100 kW
Based on current cost [JPYen]	37.74 (A)	38.05	38.28	38.58	38.73	38.98	39.21	39.47	39.74	40.04
Scenario (1) [JPYen]	28.59 (B)	28.75	29.00	29.20	29.40	29.61	29.80	30.06	30.22	30.49
Scenario (2) [JPYen]	37.61 (C)	37.77	37.83	37.95	38.11	38.18	38.38	38.45	38.59	38.70
Scenario (3) [JPYen]	28.41	28.50	28.59	28.64	28.74	28.81	28.88	28.97	29.07	29.33 (D)

A: Base scenario with 10 kW fuel cell; B: scenario (1) with 10 kW fuel cell; C: scenario (2) with 10 kW fuel cell; D: scenario (3) with 100 kW fuel cell.

Table 14. Size of each component of the HRES in the future cost scenario.

Category	PV [kW]	Wind Turbine [kW]	Fuel Cell [kW]	Electrolyzer [kW]	H ₂ Tank [kg]	Converter [kW]
Class (A)	1782	10	10	100	20	1542
Class (B)	5008	10	10	100	20	2786
Class (C)	1782	10	10	100	20	1542
Class (D)	5148	10	100	1000	200	2785

Table 15 shows the electricity generation and COE for each component from class (A) to class (D). Based on class (D), the amount of electricity generated by each component increases in proportion to the installed capacities.

Table 15. Electricity generation from each component of the HRES in the future cost scenario.

Category	PV [MWh/Year]	Wind Turbine [MWh/Year]	Fuel Cell [MWh/Year]	Grid [MWh/Year]	COE [JPYen]
Class (A)	2500	14.5	4.6	7144	37.74
Class (B)	7026	14.5	14.3	5068	28.59
Class (C)	2500	14.5	4.6	7144	37.61
Class (D)	7223	14.5	114	4922	29.33

It can be observed that the electricity generation from the fuel cell in class (D) is substantial. Based on these results, larger capacity components can be adopted, as the installation and maintenance costs of renewable energy systems are expected to be reduced in the future. This will lead to better COE, which will contribute to the realization of a cleaner energy society.

5. Conclusions

This study proposed a grid-tied hybrid solar–wind system, which can be installed at Kyushu University’s Chikushi Campus in Kasuga, Japan. The proposed HRES is equipped with a FLC-based MPPT, which provides rapid power control with smaller oscillations under variable weather conditions. The dynamic simulation of the proposed HRES system was performed in MATLAB -Simulink. The research results indicated the FLC-based MPPT’s better performance in optimal power controlling of the HRES. According to the results, by implementing the FLC-based MPPT, about 26.2 kWh/y extra electricity can be extracted from each KW installed capacity of solar panels in the Chikushi campus.

The techno-economic analysis of the proposed system was performed in HOMER software, aiming to estimate the optimal configuration of the proposed HRES subject to satisfying the required annual load in the Chikushi campus. According to the results, the estimated value of COE for the HRES equipped with the FLC-based MPPT was lower. A sensitivity analysis was also carried out to assess the feasibility of the proposed HRES, using the future market price of renewable energy technologies in 2030. The results revealed that

the coming decline in the solar system's market cost, which is the largest energy source in the HRES, is essential for improving the COE. This study proves that larger systems can be installed if the costs of installing and maintaining renewable energy systems are reduced as expected.

Author Contributions: Conceptualization and methodology: H.F. and T.H., Investigation: T.H. and A.S.; Writing: H.F., T.H. and A.S.; Review, editing: H.F.; Supervising: H.F. All authors have read and agreed to the published version of the manuscript.

Funding: This research was supported by the Kyushu Natural Energy Promotion Organization.

Institutional Review Board Statement: Not applicable.

Informed Consent Statement: Not applicable.

Data Availability Statement: Not applicable.

Acknowledgments: The authors wish to thank the editor and the reviewers for their contributions on the paper.

Conflicts of Interest: The authors declare no conflict of interest

Nomenclature

ACO	Ant Colony Optimization
ANN	Artificial Neural Networks
CS	Cuckoo Search
DFOA	Dragonfly Optimization Algorithm
FSCC	Fractional Short Circuit Current
FLC	Fuzzy Logic Control
GWO	Grey Wolf Optimization
HHO	Harris Hawk Optimization
HCS	Hill Climbing Search
HRES	Hybrid Renewable Energy System
INC	Incremental Conductance
ILC	Iterative Learning Controller
IGBT	Insulated-Gate Bipolar Transistor
LCOE	Levelized Cost of Electricity
MPPT	Maximum Power Point Tracking
MPP	Maximum Power Point
NB	Negative Big
NSNPC	Negative SmallNet Present Value
PSO	Particle Swarm Optimization
P&O	Perturbation and Observation
PWM	Pulse width modulation
PS	Positive Small
PBPID	Positive BigProportional–Integral–Derivative
RBFN	Radial Basis Function Network
RSMC	Robust Sliding Mode Control
SMC	Sliding Mode Controller
SIFL	Speed-Control and Single Input Fuzzy Logic
TEA	Techno-Economic Analysis
ZE	Zero

References

1. McLellan, B.C.; Zhang, Q.; Utama, N.A.; Farzaneh, H.; Ishihara, K.N. Analysis of Japan's post-Fukushima energy strategy. *Energy Strat. Rev.* **2013**, *2*, 190–198. [[CrossRef](#)]
2. Agency for Natural Resources and Energy. *Japan's Energy*; 2019. Available online: https://www.enecho.meti.go.jp/en/category/brochures/pdf/japan_energy_2019.pdf (accessed on 14 January 2021).
3. Farzaneh, H. *Devising a Clean Energy Strategy for Asian Cities*; Springer Nature: Singapore, 2018.

4. Esteban, M.; Portugal-Pereira, J.; McLellan, B.C.; Bricker, J.; Farzaneh, H.; Djalilova, N.; Ishihara, K.N.; Takagi, H.; Roeber, V. 100% renewable energy system in Japan: Smoothing and ancillary services. *Appl. Energy* **2018**, *224*, 698–707. [[CrossRef](#)]
5. Yoshida, Y.; Keisuke, N.; Farzaneh, H. Optimal Design and Operation of a Residential Hybrid Microgrid System in Kasuga City. In *Sustainable Production, Life Cycle Engineering and Management*; J.B. Metzler: Stuttgart, Germany, 2021; pp. 499–512.
6. Takatsu, N.; Farzaneh, H. Techno-Economic Analysis of a Hybrid Solar-Hydrogen-Biomass System for Off-Grid Power Supply. In *Sustainable Production, Life Cycle Engineering and Management*; J.B. Metzler: Stuttgart, Germany, 2021; pp. 483–497.
7. Roth, A.; Boix, M.; Gerbaud, V.; Montastruc, L.; Etur, P. A flexible metamodel architecture for optimal design of Hybrid Renewable Energy Systems (HRES)—Case study of a stand-alone HRES for a factory in tropical island. *J. Clean. Prod.* **2019**, *223*, 214–225. [[CrossRef](#)]
8. Yoshida, Y.; Farzaneh, H. Optimal design of a stand-alone residential hybrid microgrid system for enhancing renewable energy deployment in Japan. *Energies* **2020**, *13*, 1737. [[CrossRef](#)]
9. Takatsu, N.; Farzaneh, H. Techno-Economic Analysis of a Novel Hydrogen-Based Hybrid Renewable Energy System for Both Grid-Tied and Off-Grid Power Supply in Japan: The Case of Fukushima Prefecture. *Appl. Sci.* **2020**, *10*, 4061. [[CrossRef](#)]
10. Shaqour, A.; Farzaneh, H.; Yoshida, Y.; Hinokuma, T. Power control and simulation of a building integrated stand-alone hybrid PV-wind-battery system in Kasuga City, Japan. *Energy Rep.* **2020**, *6*, 1528–1544. [[CrossRef](#)]
11. Wu, G.; Kodama, S.; Ono, Y.; Monma, Y. A hybrid microgrid system including renewable power generations and energy storages for supplying both the DC and AC loads. In Proceedings of the 2012 International Conference on Renewable Energy Research and Applications (ICRERA), Nagasaki, Japan, 11–14 November 2012; pp. 1–5.
12. Sugimura, M.; Senjyu, T.; Krishna, N.; Mandal, P.; Abdel-Akher, M.; Hemeida, A.M. Sizing and Operation Optimization for Renewable Energy facilities with Demand Response in Micro-grid. In Proceedings of the 2019 20th International Conference on Intelligent System Application to Power Systems (ISAP), New Delhi, India, 10–14 December 2019; pp. 1–5.
13. Heydari-Doostabad, H.; Keypour, R.; Khalghani, M.R.; Khooban, M.H. A new approach in MPPT for photovoltaic array based on Extremum Seeking Control under uniform and non-uniform irradiances. *Sol. Energy* **2013**, *94*, 28–36. [[CrossRef](#)]
14. García, A.E.; Tutor, A.; Ángel, J.; Ramírez, O. *Maximum Power Point Tracking Algorithms for Solar Photo-Voltaic Systems*; Universidad Politécnica de Madrid: Madrid, Spain, 2017.
15. Zhang, X.; Gamage, D.; Wang, B.; Ukil, A. Hybrid Maximum Power Point Tracking Method Based on Iterative Learning Control and Perturb & Observe Method. *IEEE Trans. Sustain. Energy* **2021**, *12*, 659–670. [[CrossRef](#)]
16. Messalti, S.; Harrag, A.; Loukriz, A. A new variable step size neural networks MPPT controller: Review, simulation and hardware implementation. *Renew. Sustain. Energy Rev.* **2017**, *68*, 221–233. [[CrossRef](#)]
17. Ahmed, J.; Salam, Z. A Modified P&O Maximum Power Point Tracking Method With Reduced Steady-State Oscillation and Improved Tracking Efficiency. *IEEE Trans. Sustain. Energy* **2016**, *7*, 1506–1515. [[CrossRef](#)]
18. Mei, Q.; Shan, M.; Liu, L.; Guerrero, J.M. A Novel Improved Variable Step-Size Incremental-Resistance MPPT Method for PV Systems. *IEEE Trans. Ind. Electron.* **2011**, *58*, 2427–2434. [[CrossRef](#)]
19. Sher, H.A.; Murtaza, A.F.; Noman, A.; Addoweesh, K.E.; Al-Haddad, K.; Chiaberge, M. A New Sensorless Hybrid MPPT Algorithm Based on Fractional Short-Circuit Current Measurement and P&O MPPT. *IEEE Trans. Sustain. Energy* **2015**, *6*, 1426–1434. [[CrossRef](#)]
20. Kumar, K.; Ramesh Babu, N.; Prabhu, K.R. Design and analysis of RBFN-based single MPPT controller for hybrid solar and wind energy system. *IEEE Access* **2017**, *5*, 15308–15317. [[CrossRef](#)]
21. Zebraoui, O.; Bouzi, M. Improved MPPT controls for a standalone PV/wind/battery hybrid energy system. *Int. J. Power Electron. Drive Syst. (IJPEDS)* **2020**, *11*, 988–1001. [[CrossRef](#)]
22. Mansoor, M.; Mirza, A.F.; Ling, Q. Harris hawk optimization-based MPPT control for PV systems under partial shading conditions. *J. Clean. Prod.* **2020**, *274*, 122857. [[CrossRef](#)]
23. Benlahbib, B.; Bouarroudj, N.; Mekhilef, S.; Abdeldjalil, D.; Abdelkrim, T.; Bouchafaa, F.; Lakhdari, A. Experimental investigation of power management and control of a PV/wind/fuel cell/battery hybrid energy system microgrid. *Int. J. Hydrog. Energy* **2020**, *45*, 29110–29122. [[CrossRef](#)]
24. Priyadarshi, N.; Ramachandramurthy, V.K.; Padmanaban, S.; Azam, F. An Ant Colony Optimized MPPT for Standalone Hybrid PV-Wind Power System with Single Cuk Converter. *Energies* **2019**, *12*, 167. [[CrossRef](#)]
25. Phan, B.C.; Lai, Y.C. Control strategy of a hybrid renewable energy system based on reinforcement learning approach for an isolated Microgrid. *Appl. Sci.* **2019**, *9*, 4001. [[CrossRef](#)]
26. Hadjaissa, A.; Ameer, K.; Boutoubat, M. A WCA-based optimization of a fuzzy sliding-mode controller for stand-alone hybrid renewable power system. *Soft Comput.* **2018**, *23*, 7831–7842. [[CrossRef](#)]
27. Tazay, A.F.; Ibrahim, A.M.A.; Noureldeen, O.; Hamdan, I. Modeling, Control, and Performance Evaluation of Grid-Tied Hybrid PV/Wind Power Generation System: Case Study of Gabel El-Zeit Region, Egypt. *IEEE Access* **2020**, *8*, 96528–96542. [[CrossRef](#)]
28. Laxman, B.; Annamraju, A.; Srikanth, N.V. A grey wolf optimized fuzzy logic based MPPT for shaded solar photovoltaic systems in microgrids. *Int. J. Hydrog. Energy* **2021**, *46*, 10653–10665. [[CrossRef](#)]
29. Li, X.; Wen, H.; Hu, Y.; Jiang, L. A novel beta parameter based fuzzy-logic controller for photovoltaic MPPT application. *Renew. Energy* **2019**, *130*, 416–427. [[CrossRef](#)]
30. Keyrouz, F. Enhanced Bayesian Based MPPT Controller for PV Systems. *IEEE Power Energy Technol. Syst. J.* **2018**, *5*, 11–17. [[CrossRef](#)]

31. ECO-WORTHY. Available online: <https://www.eco-worthy.com> (accessed on 24 February 2021).
32. Algarín, C.R.; Fuentes, R.L.; Castro, A.O. Implementation of a cost-effective fuzzy MPPT controller on the Arduino board. *Int. J. Smart Sens. Intell. Syst.* **2018**, *11*, 1–10. [[CrossRef](#)]
33. Lee, J.; Kim, Y.C. Fuzzy Logic Based Maximum Power Point Tracking Algorithm for Photovoltaic Power Generation System. *J. Green Eng.* **2016**, *6*, 403–426.
34. Shahzad, M.K.; Zahid, A.; Rashid, T.U.; Rehan, M.A.; Ali, M.; Ahmad, M. Techno-economic feasibility analysis of a solar-biomass off grid system for the electrification of remote rural areas in Pakistan using HOMER software. *Renew. Energy* **2017**, *106*, 264–273. [[CrossRef](#)]
35. HOMER–Hybrid Renewable and Distributed Generation System Design Software. Available online: <https://www.homerenergy.com> (accessed on 24 February 2021).
36. Hydrogen and Fuel Cells in Japan. 2019. Retrieved from EU-Japan Centre for Industrial Cooperation Web-site. Available online: https://www.eu-japan.eu/sites/default/files/publications/docs/hydrogen_and_fuel_cells_in_japan.pdf (accessed on 14 January 2021).